Cell Reports

Article

High-content, targeted RNA-seq screening in organoids for drug discovery in colorectal cancer

Graphical abstract

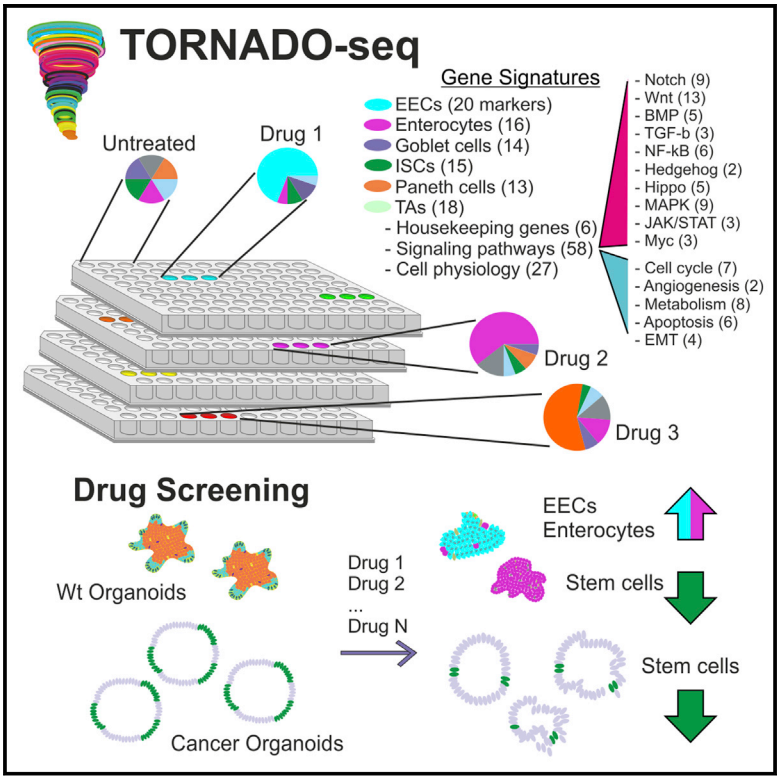

Highlights

- TORNADO-seq (targeted organoid sequencing) for affordable high-content screens
- Rapid and reliable quantification of cell types and differentiation states
- Drug screen in normal and cancer organoids found differentiation-inducing drugs

Authors

Maxim Norkin, Paloma Ordóñez-Morán, Joerg Huelsken

Correspondence

joerg.huelsken@epfl.ch

In brief

Norkin et al. develop high-throughput, high-content organoid screening for the systematic, large-scale, and quantitative analysis of complex biological systems involving many cell types and alternative activation states. Targeted RNA-seq analysis of signature gene sets allows the classification of responses to large collections of drugs or other pertubagens at minimal cost.

Norkin et al., 2021, Cell Reports *35*, 109026
April 20, 2021
https://doi.org/10.1016/j.celrep.2021.109026

CellPress

Cell Reports

CellPress
OPEN ACCESS

Article

High-content, targeted RNA-seq screening in organoids for drug discovery in colorectal cancer

Maxim Norkin,[1] Paloma Ordóñez-Morán,[2] and Joerg Huelsken[1,3,*]
[1]Swiss Institute for Experimental Cancer Research (ISREC), École Polytechnique Fédérale de Lausanne-(EPFL-SV), 1015 Lausanne, Switzerland
[2]Department of Cancer and Stem Cells, School of Medicine, Biodiscovery Institute, University of Nottingham, Nottingham NG7 2RD, UK
[3]Lead contact
*Correspondence: joerg.huelsken@epfl.ch
https://doi.org/10.1016/j.celrep.2021.109026

SUMMARY

Organoids allow the recapitulation of intestinal homeostasis and cancerogenesis *in vitro*; however, RNA sequencing (RNA-seq)-based methods for drug screens are missing. We develop targeted organoid sequencing (TORNADO-seq), a high-throughput, high-content drug discovery platform that uses targeted RNA-seq to monitor the expression of large gene signatures for the detailed evaluation of cellular phenotypes in organoids. TORNADO-seq is a fast, highly reproducible time- and cost-effective ($5 per sample) method that can probe cell mixtures and their differentiation state in the intestinal system. We apply this method to isolate drugs that enrich for differentiated cell phenotypes and show that these drugs are highly efficacious against cancer compared to wild-type organoids. Furthermore, TORNADO-seq facilitates in-depth insight into the mode of action of these drugs. Our technology can easily be adapted to many other systems and will allow for more systematic, large-scale, and quantitative approaches to study the biology of complex cellular systems.

INTRODUCTION

Colorectal cancer (CRC) is among the 3 most commonly diagnosed cancers and one of the major causes of cancer-related morbidity and mortality (Haggar and Boushey, 2009). In particular, late-stage and metastatic tumors remain challenging to treat. Novel drug-based therapies are urgently needed, since despite many attempts, successful surgery still contributes the most to patient outcomes. CRC tumors were shown to retain partially differentiated, enterocyte- and goblet-like phenotypes, as well as stem-like epithelial phenotypes, indicating the existence of rudimentary differentiation programs (Li et al., 2017). In particular, the frequency of stem-like cells has been linked to tumor maintenance, progression, and metastasis (Fumagalli et al., 2020). We have recently established differentiation therapy as an alternative modality for CRC, which targets these stem-like cells and induces their differentiation, resulting in tumor regression in patient-derived xenotransplants and mouse models of intestinal cancer (Figure 1A; Ordóñez-Morán et al., 2015). Intestinal epithelial differentiation comprises a complex program that involves at least 8 different cellular phenotypes and has been modeled recently using organoid systems (Yin et al., 2014). Intestinal organoids are derived from intestinal stem cells (ISCs), which expand and differentiate in an extracellular matrix to contain all of the cell types present in the gut epithelium. This highly representative model has been used to study development, mechanisms of differentiation, and rare epithelial phenotypes of the intestine (Yin et al., 2014; Basak et al., 2017). For example, it has been shown that the inhibition of Wnt and the activation of Notch signaling induce absorptive lineage differentiation, while the inhibition of Wnt, Notch, and epidermal growth factor receptor (EGFR) signaling induces enteroendocrine cell (EEC) fate (Basak et al., 2017). Furthermore, organoids can be derived from CRC patient samples (patient-derived organoids, PDOs), and have been used for personalized therapy approaches with a limited number of drugs (10–60 PDOs and 1–83 compounds; Gao et al., 2015; van de Wetering et al., 2015; Verissimo et al., 2016; Schütte et al., 2017; Tashiro et al., 2017). These assays typically measured cell growth/death, which provided only limited information on the biology of drug action. Drug screens with CRC cell lines often covered a larger number of drugs; however, these were still limited by a small number of measured parameters such as the activity of 1–3 pathway reporters (Miyamoto et al., 2019; Zhan et al., 2019)

Here, we developed a high-content, high-throughput screening system in organoids to identify small-molecule drugs that are able to induce the differentiation of intestinal wild-type (WT) and cancer cells. This is achieved by RNA expression analysis quantifying a large number of cell-type-specific genes, followed by deconvolution methods to infer cell-type composition. As a high-content technology, mRNA expression analysis offers several advantages such as precision, scalability, and sensitivity

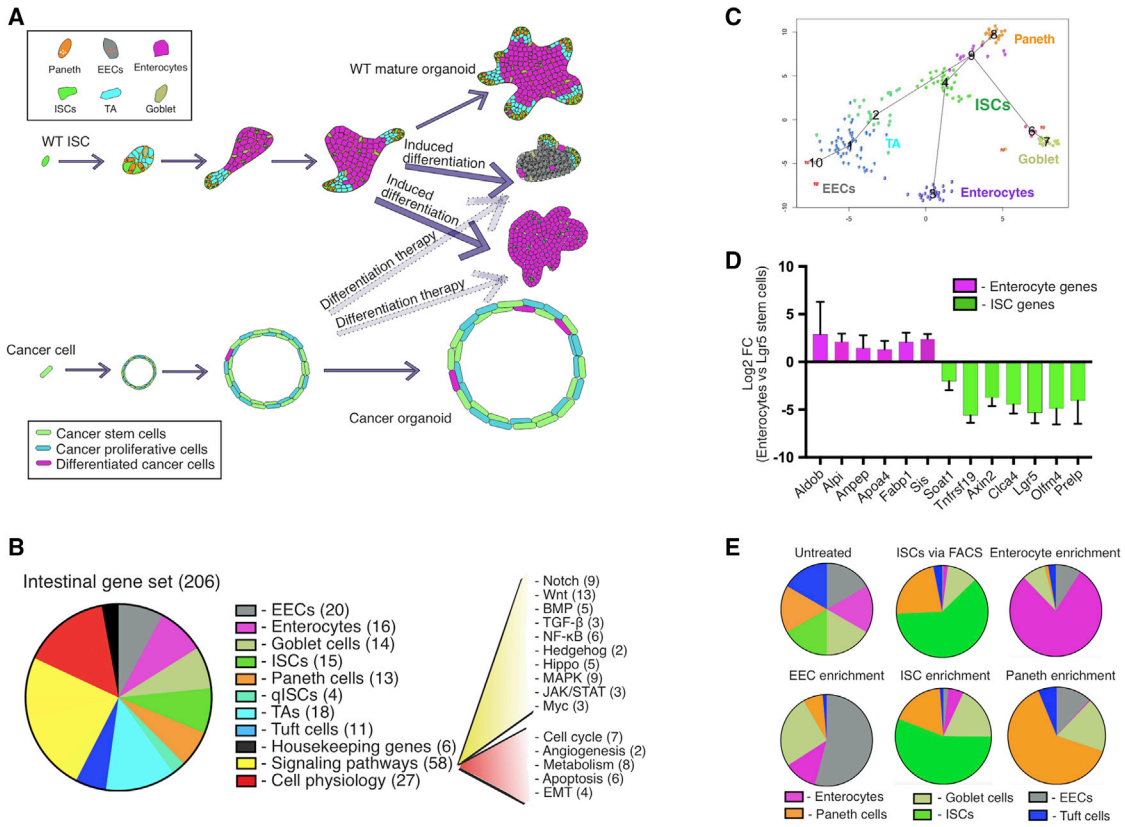

Figure 1. Differentiation therapy and the establishment of a representative intestinal gene set

(A) Schematic representation of the differentiation process in WT organoids and differentiation therapy in cancer.

(B) Composition of the selected 206 gene set for the assay.

(C) Clustering of single intestinal epithelial cells based on the expression of our 206 gene signature into the different intestinal populations using the StemID2 algorithm (Grün et al., 2015). Cluster numbers are depicted in black; each dot corresponds to 1 cell. Cluster 1, enterocyte progenitors; cluster 2, TA; cluster 3, enterocytes; cluster 4, ISCs; cluster 5, EECs (not depicted); cluster 6, goblet cells; cluster 7, goblet cells; cluster 8, Paneth cells; cluster 9, Paneth cells; cluster 10, EECs.

(D) qPCR data on organoids enriched for stem cells or absorptive enterocytes. Log2FC (fold change) are shown, error bars represent SD values. Number of replicates n = 3.

(E) qPCR data on WT organoid samples enriched for certain cell populations represented as pie charts. Each sector of a pie represents 1 cell population, which was detected in the sample based on the expression of 5–10 specific marker genes. Untreated organoids are shown as a pie with an equal percentage of each cell population (artificial cell composition is depicted). FC of each population in the sample composition is converted to the percentages represented as sectors in the pies. Organoid culture conditions: enterocytes, IWP-2 and valproic acid (VPA); ISCs, CHIR and VPA; Paneth, DAPT; EECs, DAPT, IWP-2, and gefitinib; 2 days' treatment.

over other methods such as those that are antibody or reporter based. Until now, no next-generation sequencing (NGS)-based screens in organoids were developed due to the technical limitations imposed by organoids growing in solidified drops of Matrigel and the cost of classical RNA sequencing (RNA-seq) assays. Furthermore, eukaryotic transcriptomes exhibit a wide dynamic range of gene expression levels, with a minority of highly expressed genes making up the majority of RNA molecules within a cell. Classical RNA-seq insufficiently samples weakly expressed transcripts, resulting in sparse sequence coverage and uncertain quantification. By using oligonucleotide primers to restrict analysis to selected genes, targeted RNA-seq improves sequencing read coverage, allowing sensitive and reliable gene expression measurement over an extended dynamic range. In addition, in combination with multiplex library preparation, the increased efficiency of targeted RNA-seq can also reduce costs by increasing the number of conditions analyzed in parallel.

For the analysis of complex phenotypes such as multi-lineage differentiation, there is a need for high-content assays, which not only enable drug discovery but also provide insight into biological mechanisms. Here, we developed a high-content assay to measure gene expression profiles that provide information on the frequency of all possible intestinal cellular phenotypes, major signaling pathways, and general cell physiology, detecting 206 carefully selected genes in either WT or cancer intestinal organoids. Our assay is cost-efficient and allows the analysis of thousands of treated samples in 1 sequencing reaction, while achieving high efficiency and reproducibility. Our technology can be easily adapted to answer many other biological questions and will allow a more systematic, large-scale, and quantitative approach in a number of fields such as developmental biology,

physiology, pharmacology, and personalized medicine, which involve dynamic, multicellular *in vitro* systems.

RESULTS

Screen design and validation

To cover the different intestinal cell phenotypes, we selected 111 marker genes for these 8 populations: ISCs, transient amplifying (TA) cells, absorptive enterocytes (E), EECs, goblet cells, Paneth cells (P), tuft cells, and quiescent ISCs (qISCs) (Figure 1B). These marker genes were selected from published datasets of bulk RNA-seq and single-cell RNA-seq of primary intestinal cell suspensions and organoid cultures, which were further enriched by fluorescence-activated cell sorting (FACS) or *in vitro* differentiation protocols (please see Table S1 for the full list of studies; Basak et al., 2017; Grün et al., 2015, 2016). We further included 58 genes reporting on major signaling pathways (Notch, Wnt, Hedgehog, Hippo, bone morphogenic protein/transforming growth factor β [BMP/TGF-β], nuclear factor κB [NF-κB], and growth factor signaling), 27 genes of general cell physiology (cell cycle, metabolism, angiogenesis, apoptosis, epithelial-mesenchymal transition), and 6 housekeeping genes expressed in the whole intestine. The complete list of 206 genes was selected based on uniqueness, expression level, reproducibility, and multi-set intersection (Table S1). The clustering of single cells into the different intestinal populations based on the expression of only this gene list produced comparable results as the full transcriptome with 90% overlap in classifications of cell identity using the StemID2 (Grün et al., 2015, 2016) or the Seurat (Butler et al., 2018) algorithm, confirming the performance of the selected gene set (Figures 1C and S1A).

Primers were designed using standard primer design guidelines considering secondary structures and primer dimers using established software for multiplex PCR design (for details, please see Method details). To validate primers for our gene list, we performed qPCRs on different cell populations of the murine small intestine. Cells were either sorted by FACS (Lgr5-GFP^{+} ISCs) or induced to differentiate into E, ISC, P, or EEC lineages in organoid culture using published media conditions (Yin et al., 2014; Basak et al., 2017). Our results showed robust upregulation of lineage-specific markers in the respective populations; for example, the stem cell signature was highly enriched in Lgr5^{+} ISCs but lost in absorptive enterocytes, and vice versa, the enterocyte-specific signature was enriched in organoids induced to differentiate into absorptive enterocytes and barely detectable in ISCs (Figure 1D). Such validation was performed for all of the major lineages (Figure 1E).

To implement this gene set for high-throughput screening, we developed and validated a targeted RNA-seq method (Figures 2A and 2B) that we called TORNADO-seq (targeted organoid sequencing). Briefly, we isolated mRNA of treated organoids from 1 well of a 96-well plate (~10,000 cells) using oligo(dT) magnetic beads and synthesized cDNA in a reverse transcription (RT) reaction using a mixture of 206 gene-specific reverse primers carrying a unique molecular identifier (UMI) and a common part needed for subsequent amplification steps. The obtained cDNA was amplified in a 1st stage PCR with 1 common reverse primer and a mixture of 206 gene-specific forward primers (containing a second common part) (Figure 2A). The obtained products were barcoded in a 2nd stage PCR and pooled for library preparation and sequencing (Figure 2A). After analysis of the initial targeted RNA-seq results, primers showing inadequate or unspecific amplification were re-designed and substituted with new pairs. In addition, primer concentrations were adapted so that amplicons of high abundance were diluted, enabling the enrichment of sequencing read coverage for weakly expressed genes and more precise quantification. In total, 3 iterations of primer re-design and concentration adjustment were performed to optimize the assay. The final setup provides excellent reproducibility, showing a Pearson's correlation coefficient of $r > 0.95$ based on raw read counts of untreated biological replicates (Figure S1B). Comparison of RNA-seq and qPCR-based quantification of gene expression revealed a high correlation confirming the accuracy of our method with a Pearson's correlation coefficient of $r = 0.79$ (Figure 2C). We sequenced >3,000 samples, with an average sequencing depth of 70,000 reads per sample. The average read coverage was 370 reads per gene, with 50% of the genes having >100 reads (counts) per gene and >80% of genes having >10 reads per gene (Figure 2D). The average mapping efficiency to the targeted gene signature was 70% and reached 95% as a function of mRNA quantity. The duplication rate as assessed by UMIs varied between genes and equaled 2.2 transcripts per UMI on average. Due to the improved uniformity of read distributions by TORNADO-seq compared to conventional RNA-seq technology, we can use a moderate sequencing depth (50,000 reads per sample), allowing the analysis of more samples in parallel and reducing the total cost of our assay (including reagents for cell culture, sequencing library preparation, and sequencing cost) to $5 per sample.

Identification of differentiation-inducing drugs in WT intestinal organoids

To identify small-molecule drugs that induce intestinal epithelial differentiation in organoids from WT mice, we assayed 320 compounds from a library of US Food and Drug Administration (FDA)-approved drugs. Our screen identified 56 drugs as potential hits using a threshold of at least 5 significantly altered, differentially expressed (DE) genes ($|\log2FC| > 1$, $padj < 0.05$) based on obtained gene expression profiles (Figure 3A). The screen exhibited good reproducibility, showing a Pearson's correlation coefficient of $r = 0.93$ based on raw read counts across all of the drugs (Figure S1C) and $r = 0.65$ for top drug hits using fold change (FC) values over untreated samples. Among those potential hits were substances already used for the treatment of colon cancer (itraconazole; Buczacki et al., 2018), pyrvinium (Wiegering et al., 2014; Li et al., 2014), tubulin inhibitors (bendazoles, colchicine), and cytotoxic drugs known to affect general cell physiology (antimetabolites gemcitabine, azaguanine, mercaptopurine, floxuridine; topoisomerase inhibitors; and cytotoxic antibiotics: anthracyclines and antimycins). Interestingly, our screen identified several drug candidates such as antipsychotic phenothiazines, cholesterol-lowering statins, antimycotic conazoles, selective estrogen-receptor modulators (SERMs), glucocorticoids, and antihistamines. Supervised clustering based on cell-type-specific genes identified common gene expression alterations that resulted in 5 distinct clusters of drugs (Figure 3A).

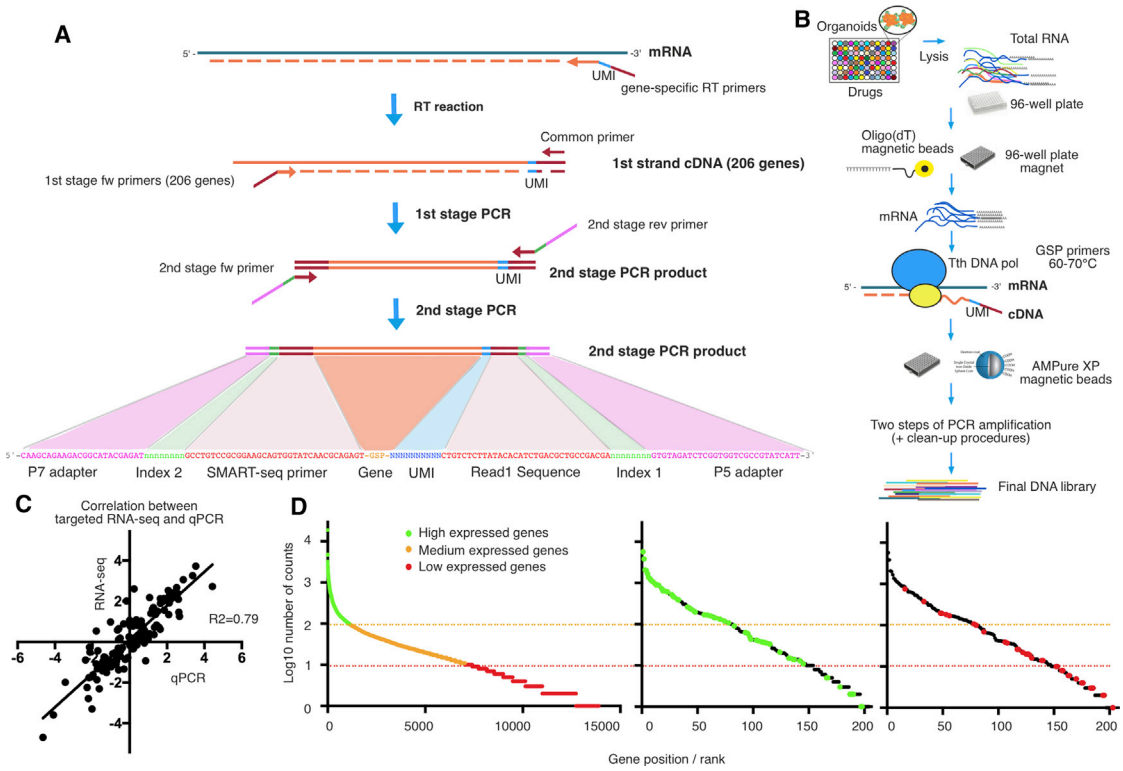

Figure 2. Schematic representation of library preparation for targeted RNA sequencing

(A) cDNA was synthesized from polyA mRNA in an RT reaction using a mixture of 206 gene-specific reverse primers (GSP) carrying a UMI and a common sequence (part of Illumina Read1 sequence) needed for further amplification steps. The obtained cDNAs were further amplified in a 1st stage PCR with 1 common primer and the mixture of 206 gene-specific forward primers (carrying a 2nd common part derived from switch mechanism at the 5′ end of RNA templates sequencing [SMART-seq]). The obtained products were barcoded in a 2nd stage PCR using a set of forward and reverse primers (carrying index1 and index2, and P5 and P7 adapters for Illumina sequencing).

(B) Schematic view of high-throughput processing of drug-treated intestinal organoids. Organoids were seeded in a 96-well plate format in Matrigel, drug treated, and then lysed. mRNA was isolated from lysates using oligo-dT magnetic beads in a 96-well plate format. Tth DNA polymerase was used for the RT reaction, and cDNA was purified with AMPure XP magnetic beads. After 2 rounds of PCR amplification, an additional clean-up procedure with AMPure XP magnetic beads was performed, and final libraries were pooled and purified twice on 2% agarose gel (not shown).

(C) Pearson's correlation of mRNA quantification between qPCR and targeted RNA-seq. Thirty random genes were chosen for the comparison. Log2FC values are represented.

(D) Left: conventional RNA-seq data of untreated organoids from repository GSM2358985. Three million reads distribution, 14,000 genes represented. Genes from our 206 gene signature with high, mid-, and low expression are represented by green, orange, and red dots, respectively. Right: targeted RNA-seq of untreated organoids; 40,000 reads distribution. High (green) and low (red) expressed genes (colors as quantified in 2 dimensions [2D]) are depicted with their expression rank quantified by our targeted RNA-seq method. The number of reads was normalized by the combined number of all 206 selected genes. The number of reads between conventional and targeted RNA-seq was normalized by the combined expression of the 206 selected genes.

All cytotoxic compounds (cluster WT-1) suppressed ISC, TA, and cell-cycle signatures as expected. At the same time, the more potent anthracyclines (epirubicin, doxorubicin, daunorubicin) exhibited a very specific pattern and led to a relative increase in absorptive enterocyte-specific genes. Loss of ISCs and increased enterocytic differentiation was confirmed by fatty acid binding protein 1 (FABP1) immunofluorescence staining and cytometry for Lgr5-GFP (Figures 4A and 4C). This is likely an indirect effect since these compounds deplete proliferative cells (Figure 4C), causing a relative accumulation of differentiated cells, most prominently absorptive enterocytes, as the most frequent differentiated cell type in organoids. When analyzing the microscopy images that were taken before harvesting the organoids for RNA isolation, cell death occurred twice as frequently for cytotoxic compounds compared to non-toxic compounds (Figures S2C and S2D). We excluded the possibility that dead cells affected the measured RNA expression changes (Figures S2A and S2B). Importantly and in contrast to the cytotoxic drugs of cluster WT-1, the remaining clusters (WT-2–WT-5) induced different responses. The vast majority of drugs in cluster WT-2 (statins, SERMs, and phenothiazines) decreased enterocyte frequencies; upregulated markers of other differentiated cell phenotypes such as EECs, goblet, or tuft cells; and decreased proliferation-related genes to a lesser extent. In particular, statins and phenothiazines were characterized by a large increase in EEC markers. Cluster WT-3 contained glucocorticoids that induced an inflammatory signature evidenced by the upregulation of *Apoa4*, *Cdkn1a*, *Pdlim2*, *Prpa1*, and *Nfkbia*, and the downregulation of *Clca4*, *Sis*, *Cdc25c*, and *Cck*. This more global pattern in response to

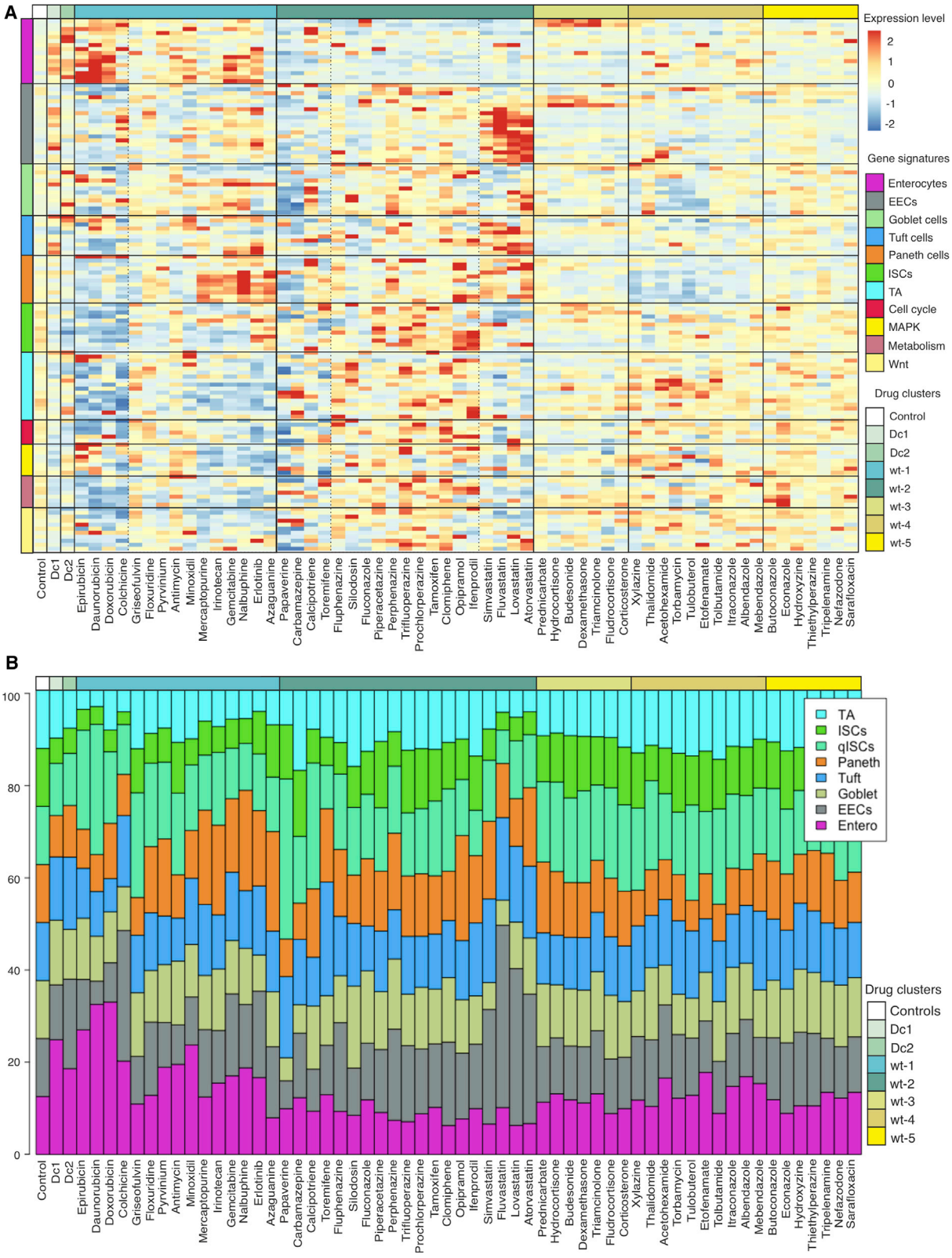

(legend on next page)

glucocorticoids was also observed in the Connectivity Map (CMAP) database, which supports the validity of our assay (Figure S3A). Drug cluster WT-4 showed a robust downregulation of P cells, while drugs from cluster WT-5, which included conazoles, altered only a few differentiation-associated genes. Phenotypic changes reported in the screen were validated by qPCR for some of these clusters, confirming the robustness of our method (Figure S3C).

The majority of potential drug hits was further evaluated based on the upregulation or downregulation of at least 5 differentiation or stem cell genes, respectively ($|log2FC| > 1$, $padj < 0.05$), which resulted in 27 drugs classified as differentiation inducing. Furthermore, cell-type enrichment analysis revealed that some of these drugs induced differentiation to a specific cell type. We identified lovastatin, atorvastatin, perphenazine, and trifluoperazine to specifically induce EEC enrichment as well as P cell markers. All 4 drugs do not upregulate absorptive enterocyte-specific genes, which is in contrast to another EEC induction cocktail (Figure 3A, Dc2) suggested earlier (Basak et al., 2017). This cocktail has broader effects on intestinal differentiation, including the induction of enterocytes and goblet cells (Figures 4A and 4B). Moreover, we also identified drugs that specifically deplete certain cell types; for example, silodosin depleted enterocytes, while tulobuterol, xylazine, and other drugs from cluster WT-4 depleted P cell markers (Figure 3A). Cell-type enrichments for all drugs are quantified and summarized in Figure 3B and Table S2. For selected drugs, treatment effects were validated by orthogonal assays (Figure 4). We used immunofluorescence analysis of FABP1 to quantify enterocytes and of chromogranin A (CHGA) and serotonin to detect EECs. Furthermore, we used flow cytometry to measure intestinal stem cells via the Lgr5-GFP allele and cell death via DAPI. Finally, we used the histology stains Sirius Red and periodic acid-Schiff (PAS) to identify P and goblet cells, respectively. These assays confirmed changes in cell lineage frequency in line with what we had measured using our targeted RNA-seq approach. For example, statins increased secretory lineages such as enteroendocrine and P cells and decreased stem cell frequency, while daunorubicin increased enterocytes and decreased stem and EEC frequencies.

Comprehensive analysis of drug-induced differentiation patterns reveals connections between cellular phenotypes and signaling pathways in WT organoids

One of the advantages of TORNADO-seq is the possibility of discovering potential crosstalk between the various signaling pathways and cell types by identifying the frequent co-regulation of genes over many treatment conditions. We analyzed these possible connections using correlograms (Figure 5A) to directly show such gene-gene correlations (Figure S4). We observed that absorptive enterocyte differentiation strongly correlates with the downregulation of ISCs and TAs as well as proliferative signatures. Differentiation into EEC, tuft, goblet, and P cells is highly interconnected, which is in line with their placement in the secretory lineage with generation from a common, secretory lineage progenitor cell. The same applies to signaling pathways: Wnt, Myc, and cell-cycle genes show high correlation, consistent with c-Myc as a known downstream target of the Wnt pathway and the role of this pathway in driving intestinal proliferation and cancer development. As well-known organizers of the stem cell niche in the intestine, Notch and Wnt pathways also displayed a high correlation. Furthermore, Wnt/β-catenin signaling correlated with epithelial-mesenchymal transition (EMT) as expected (Basu et al., 2018; Kim et al., 2019). Interestingly, a decrease in P cell markers was correlated with increased proliferation and Notch signaling (Figure 5A). This may be linked to the ability of P cells to de-differentiate and acquire stem-like properties upon injury (Schmitt et al., 2018). Moreover, Notch inhibition is well known to promote P cell expansion (Yin et al., 2014). *In vivo*, the intestinal epithelium is characterized by low oxygen concentrations and a decreasing oxygen gradient toward the lumen (Karhausen et al., 2004). Our analysis identified *Vegf*, a known marker of hypoxia, to anti-correlate with several differentiated lineages, including enterocytes (Figure S4). It remains to be seen to what extent oxygen concentrations may contribute to the intestinal lineage differentiation profile. In essence, TORNADO-seq identifies both known and unexpected interactions between cell states and signaling pathways, suggesting that this method can be an advantageous discovery tool for hypothesis generation in a variety of biological systems.

Evaluating differentiation-inducing drugs in cancer organoids

We compared the profiles of untreated, WT, and transformed APC^{lof}:KRAS^{G12}:TP53^{lof} (AKP) organoids, which were obtained from advanced mouse intestinal tumors (Figure 5B). As expected, in comparison to WT organoids, we observed an upregulation of proliferative signatures and a downregulation of differentiation markers in AKP organoids, which is a hallmark of advanced tumor progression. Of note, WT and cancer organoids exhibit different morphology; while WT organoids grow as budding structures, the cancer organoids form spheres (Figure 1A).

We next performed TORNADO-seq on drug-treated AKP cancer organoids, selecting only those drugs that had scored as potential hits in WT organoids. We found that over half (16 of 27) of the drugs inducing differentiation in the WT also affect AKP

Figure 3. TORNADO-seq identifies differentiation-inducing drugs in WT intestinal organoids

(A) Supervised clustering of WT treated samples based on the expression of cell-type-specific genes. Sub-clusters are depicted by vertical, dotted lines. Log10 [counts +1] values are represented. The expression level is computed as row *Z* score values. Drug cocktails (dcs) dc1 (IV) and dc2 (IDG) enrich for absorptive enterocytes and EECs (details in Method details).

(B) Calculated cell-type composition represented as stacked bar charts. Each sector of a bar represents 1 cell population that was detected in the sample based on the expression of specific marker genes. The untreated control depicts a cell-type distribution in WT organoids in which each population is of equal size to facilitate comparisons. Calculated relative FC of each population upon drug treatment was converted to bar sectors. The drug order and gene expression information are identical to those in (A).

Drug cluster color bar represented at the top of the figure.

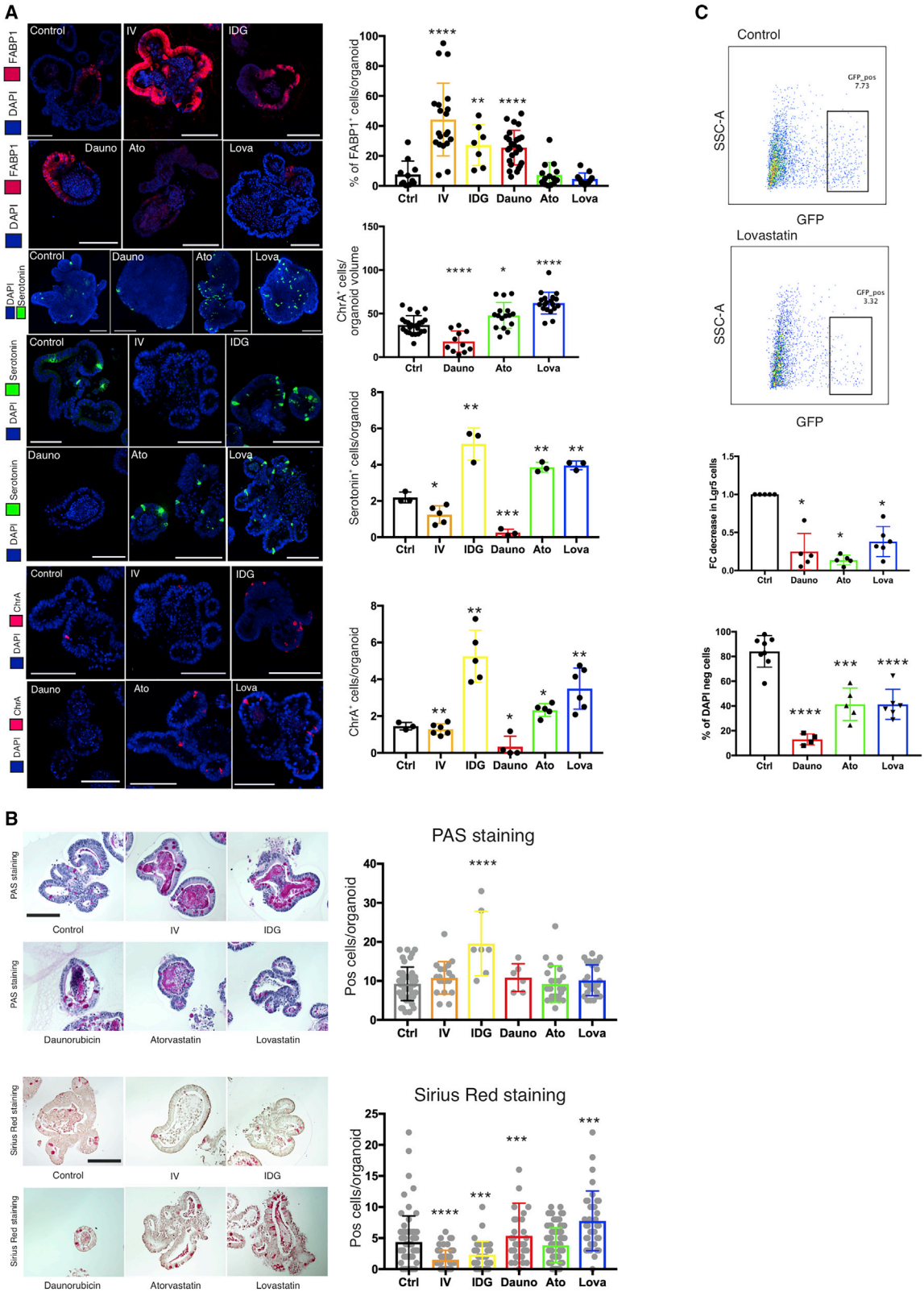

(legend on next page)

organoids (using the same criteria as for the WT: deregulation of at least 5 stem or differentiation-related genes) by inducing the loss of stem cell signatures concomitant with an upregulation of differentiation markers (Figure 6B; Table S3). Importantly, when we evaluated the full set of 320 drugs on AKP cancer organoids by morphological scoring, we obtained identical results—only drugs inducing differentiation in WT organoids targeted cancer organoids causing prominent growth arrest and cell death, while all other drugs were ineffective. This suggests that differentiation induction may be a major factor determining drug activity.

Supervised clustering (excluding the drugs of cluster WT -1, which largely contained cytotoxic drugs) revealed 3 drug clusters that resembled the clusters for WT organoids: one cluster containing tubulin inhibitors, AKP-4 (cluster 4 in the WT); a cluster containing statins, AKP-2 (cluster 2 in the WT); and a cluster containing conazoles, AKP-5 (cluster 5 in the WT; Figure 6A). The AKP-2 cluster revealed the strongest phenotype displaying a profound decline in proliferation, reduction of ISCs and Wnt signatures, and a decrease in lipid biosynthesis genes, whereas stress-response genes (*Nupr1*, *Nfkb2*) and mitogen-activated protein kinase (MAPK) signaling increased. Importantly, statins also increased the expression of differentiation genes such as tuft cell lineage markers *Krt8* and *Krt18*. The AKP-5 cluster induced a higher expression of differentiation markers, especially for goblet and P cell-specific genes (*Muc2*, *Pla2g2a*, *Clps*) and downregulated a variety of proliferation and growth-related genes. Tubulin inhibitors showed a distinct signature with a strong decrease in inflammation response genes and a moderate decrease in ISC and Wnt signaling genes. The drugs of the glucocorticoid cluster identified in the WT screens (WT -3) did not affect cancer organoids. For selected drugs, we analyzed the time dependence of the response in cancer organoids. This revealed early and late responses (Figure S5)—a transient increase in stress responses only at day 1 of treatment involving *Nupr1*, *Nfkb*, *Birc3*, and *Nfkbia*, while Wnt signaling decreased and differentiation markers increased gradually from day 0 to day 2. Overall, this analysis revealed a striking overlap of drugs affecting both WT and cancer organoids, suggesting similar modes of action of the drugs in either model.

Treatment responses of cancer organoids exhibit distinct signatures

As we have already established, untreated WT and AKP organoids display different expression profiles (Figure 5B). Correlation and differential expression analysis for treatment-responsive AKP samples (Figure S6) showed a strong reduction in many ISC genes, while goblet-specific genes (*Muc2*, *Agr2*, *Clps*) were upregulated. The evaluation of gene-gene correlations using Gene Ontology (GO) revealed 4 differentially affected groups of genes: proliferation/metabolic genes, G1/S phase genes, cell death/apoptosis genes, and inflammation/stress response genes (GO term p values 2E−7, 2E−10, 2E−6, and 2E−5, respectively; Figure S6). Interestingly, many genes from the first 3 groups were co-regulated in WT organoids (Figure S4, green circle), but in AKP organoids, they were differentially affected and each cluster of drugs (statins, conazoles, tubulin inhibitors, and cytotoxic compounds) altered a specific combination of these group of genes. While proliferation/metabolic genes were downregulated in all of the drug clusters, the G1/S phase genes were only reduced by statins. Furthermore, while statins, conazoles, and cytotoxic drugs increased inflammation genes, these were downregulated by tubulin inhibitors. Apoptosis genes were only activated by cytotoxic drugs (Figure S7A). In line with previous reports, the proliferation signature strongly anticorrelated with inflammation (Schmitt et al., 2018). Thus, gene expression profiles of treated organoids revealed only partially overlapping responses in WT versus cancer organoids.

Drug classification helps uncover the mode of action (MOA) against cancer organoids

We performed clustering of treated WT and AKP samples based on gene expression profiles using non-negative matrix factorization (NMF) and uniform manifold approximation and projection for dimension reduction (UMAP) (Figure S7B). Despite the biological differences between WT and AKP organoids, the majority of drugs targeting AKP organoids clustered similarly to the WT setting, which indicates a common MOA in both systems. Interestingly, some of the co-clustering drugs were not known to have a common MOA. For example, phenothiazines, SERM inhibitors, and antihistamines produced responses similar to those of statins and conazoles (AKP-2, AKP-5), which are well-known cholesterol-lowering agents (Figure 7A). We therefore explored phenothiazines, SERM inhibitors, and antihistamines in more detail to elucidate whether their MOA may be related to the cholesterol biosynthesis pathway. A literature search indicated that these drugs, among many other functions, can also inhibit enzymes in the cholesterol biosynthesis pathway or may alter cholesterol trafficking (Figure 7B; Adams et al., 2003; Korade et al., 2016; Wages et al., 2018; Shim et al., 2015; Moebius et al., 1997). To verify this idea, we performed rescue experiments by adding cholesterol-cyclodextrin complex to drug-treated organoids. This overcame the differentiation phenotypes produced by statins, phenothiazines, SERMs and the sigma

Figure 4. Differentiation phenotypes are confirmed by orthogonal assays

(A) Immunofluorescence staining with the indicated antibodies against FABP1, chromogranin A (CHGA), and serotonin of organoids cultured under the following conditions: IDG (IWP-2, DAPT, gefetenib) and IV (IWP-2, VPA) are known dcs (Yin et al., 2014; Basak et al., 2017); Dauno (daunorubicin), Ato (atorvastatin), and Lova (lovastatin) are drugs identified in our screen. Organoids were treated at 10 μM for 2 days in murine epidermal growth factor, murine noggin, human R-spondin-1 (ENR) medium. Scale bars, 100 μm. Average values of replicates are shown, error bars represent SD values.

(B) Periodic acid-Schiff (PAS) and Sirius Red staining for the detection of goblet and Paneth cells of organoids cultured under multiple conditions. IDG (IWP-2, DAPT, gefetenib) and IV (IWP-2, VPA) are known dcs (Yin et al., 2014; Basak et al., 2017); Dauno, Ato, and Lova are drugs identified in our screen. Organoids were treated at 10 μM for 2 days in ENR medium. Scale bars, 100 μm. Average values of replicates are shown, error bars represent SD values.

(C) Flow cytometry of organoids treated as above using the Lgr5-GFP allele to measure ISCs and DAPI to measure alive cells. Average values of replicates are shown, error bars represent SD values.

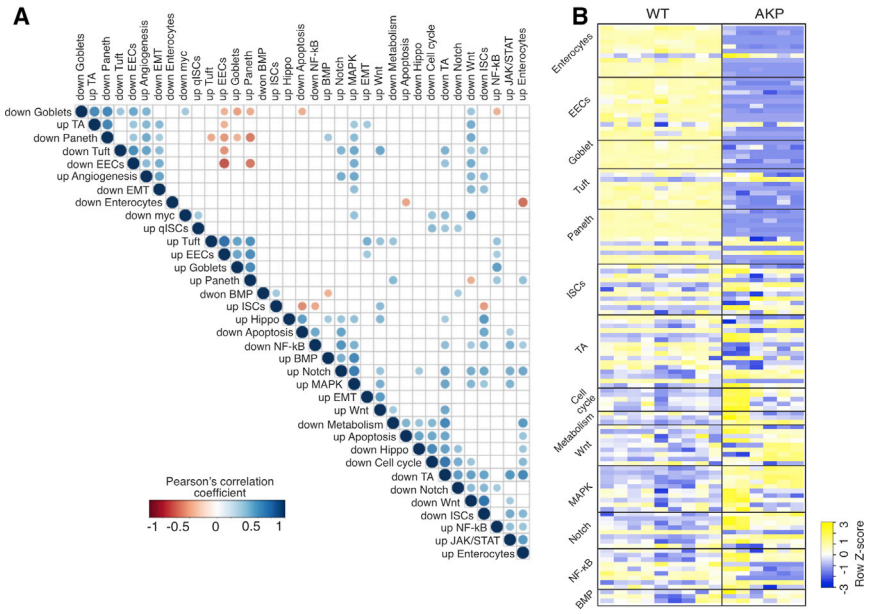

Figure 5. TORNADO-seq identifies connections between cellular phenotypes and signaling pathways in organoids

(A) Correlogram showing the correlations between various pathways and cell types in WT organoids. Correlations are computed from the gene expression profiles (Figure 1B) of organoids treated with drugs from Figure 3A (30 drugs with highest number of DE genes, see Method details) with corrplot function in R with assay p = 0.05.

(B) Expression profiles of untreated WT and AKP organoids for 130 highly expressed genes in both systems from our 206 gene set grouped by cell type or pathway/function. Log10[counts +1] values are represented. The expression level is computed as row *Z* score values.

See also Figure S4.

receptor ligands ifenprodil and opipramol (Figure 7C). Of note, this cholesterol-induced rescue was weakest for statins, and increased drug concentrations overcame cholesterol-mediated rescues. A role of cholesterol for intestinal homeostasis and cancer is supported by recent findings (Wang et al., 2018; Voorneveld et al., 2017; Miyamoto et al., 2019). Importantly, several of these drugs (ifenprodil, opipramol, perphenazine, toremifene) exhibited higher potency against AKP compared to WT organoids, suggesting a favorable therapeutic window for future application (Figure 7D). This example shows that our high-content analysis of phenotypes over a large number of drugs can help to identify MOAs and relevant pathways, which may not correspond to the expected MOA for certain drugs.

We finally evaluated drugs of the AKP-2 (statins) and AKP-5 (conazoles) clusters on human cell lines. We chose 4 cell lines representing different consensus molecular subtypes (CMSs) of CRC (Guinney et al., 2015): DLD-1 (CMS1), LS-174T (CMS2), NCI-H508 (CMS3), and HCT-116 (CMS4). More than half (10 of 17) of the drugs identified to target AKP organoids also targeted human CRC cell lines (Figure 7E; Table S4). While phenothiazines were not effective against human cell lines growing in culture medium with 10% fetal calf serum (FCS; which contains cholesterol), the statins atorvastatin and lovastatin, more potent inhibitors of cholesterol biosynthesis, showed the highest potency. Also, for the human cell lines, statin effects could be rescued by the further addition of cholesterol (data not shown) in support of their MOA. Thus, our screen identified several interesting candidates—statins, opipramol, and toremifene—for further *in vivo* validation as drug candidates for CRC therapy.

DISCUSSION

Here, we describe TORNADO-seq as a high-content approach for high-throughput drug discovery in organoids. While the majority of drug screens are based on few parameters such as the activity of signaling pathways or the measurement of cell viability, they lack the rich data required for the analysis of complex phenotypes and the MOA of drugs. We demonstrate here that TORNADO-seq is an excellent tool to overcome these limitations, for the discovery of new biological readouts, and for the analysis of multicellular phenotypes.

TORNADO-seq compares favorably with other high-content methods with respect to availability, cost, and applicability to organoid-based screens. TORNADO-seq shows high reproducibility, requires only 6 h to perform, is cost-efficient ($5 per sample, including culture, library preparation, and sequencing cost), and does not require any specialized equipment. Due to the implemented UMI counting and sequencing of amplicons, TORNADO-seq lacks PCR- and ligation-based bias and misdetections. Primer design is straightforward, needs minor optimization, and only requires moderate effort. Several high-throughput NGS methods have been established previously that are not applicable to organoid-based screens. Genome-wide RNA-seq methods require high sequencing depth for many of the weakly expressed genes relevant to our system, which increases assay cost (Ye et al., 2018; Bush et al., 2017). Other targeted approaches are based on ligation reactions between acceptor and donor probes (Simon et al., 2019; Teder et al., 2018) and require tedious optimization and troubleshooting while suffering from PCR amplification bias and difficulties in detecting weakly expressed targets (see Table S5 for comparison).

Analysis of treated WT organoids revealed known and new aspects of intestinal epithelium organization and signaling networks. Cytotoxic compounds predominantly enrich for absorptive enterocytes, which is likely related to the fast induction of cell death, and therefore loss of proliferating stem and progenitor cells, leaving behind enterocytes as the main component of intestinal organoids. A higher frequency of enterocytes was observed in daunorubicin-treated organoids by immunofluorescence analysis. In contrast, non-toxic drugs often eliminate enterocytes and enrich other cell types (e.g., EECs, goblet cells), indicating specific differentiation induction. We have also noticed a delayed phenotype with the non-toxic drugs compared

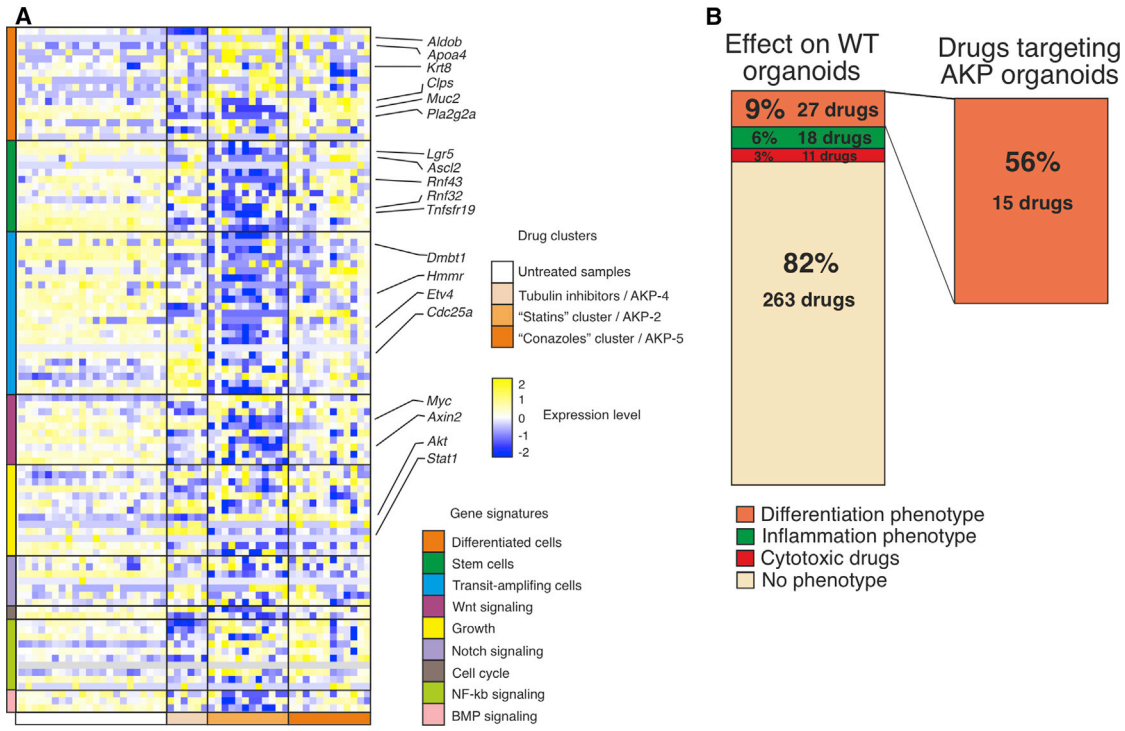

Figure 6. Differentiation-inducing drugs target AKP cancer organoids

(A) Clustering of drug-treated AKP cancer organoids based on their gene expression profiles (97 genes differentially expressed between the samples are depicted). For each drug, both replicates are displayed on the heatmap. Log10[counts +1] values are represented. The expression level is computed as row *Z* score values.
(B) Summary of drug effects on WT and AKP organoids. The left panel represents the phenotypes of all drug-treated WT organoids. The right panel represents the effect of the drugs that induce differentiation in the WT system on AKP cancer organoids. Drugs targeting AKP organoids are defined as those that downregulate/upregulate $\geq$5 stem cell/differentiation genes ($|log2FC| > 1$, padj < 0.05).

to the swift action of cytotoxic drugs, which is in line with the observation that differentiation may act over a longer timescale. We were able to identify drugs specifically enriching organoids for a certain cell type. In particular, lovastatin and trifluoperazine specifically induced EEC enrichment more precisely than previously proposed drug cocktails (Basak et al., 2017; Table S2). Observed phenotypes were detected by both bulk gene expression changes and single-cell analysis using immunofluorescence, FACS, and histology. Higher expression of EEC marker genes was caused by an increased frequency of EECs.

Importantly, we identified many drug candidates targeting colon cancer organoids, which were not described previously for CRC. Among them are antipsychotic phenothiazines, cholesterol-lowering statins, antimycotic conazoles, SERMs, and antihistamines. Based on the obtained gene expression profiles, we were able to propose and confirm MOAs for some of these drugs, which we found to act by targeting the cholesterol pathway. Several of these drugs (ifenprodil, opipramol, perphenazine, toremifene) showed a beneficial therapeutic window targeting preferentially cancer compared to WT organoids. Finally, statins, opipramol, and toremifene also targeted human CRC cell lines, warranting future *in vivo* validation.

In line with our initial hypothesis, differentiation induction seems to be a common mechanism for drugs targeting cancer organoids, as all of these drugs also induced differentiation in WT organoids. Most of these drugs trigger stem cell loss in cancer organoids, which may provide additional benefits for therapy since the stem-like population of cancer cells has been shown to have important functions in tumor maintenance, therapy resistance, and metastasis.

TORNADO-seq is a tool that can be easily optimized and adapted for mouse or human *in vitro* systems such as organoids of various tissue types, which are increasingly being developed (Schutgens and Clevers, 2020), or other differentiation-capable systems such as embryonic stem cells or induced pluripotent stem cells. It can be further combined with other perturbators such as CRISPR or expression library technologies. TORNADO-seq is therefore a promising tool in high-throughput drug discovery and translational, personalized medicine approaches, as well as for basic questions in biology that address mechanisms of development or the homeostasis of multicellular systems.

STAR★METHODS

Detailed methods are provided in the online version of this paper and include the following:

- KEY RESOURCES TABLE
- RESOURCE AVAILABILITY
  - Lead contact

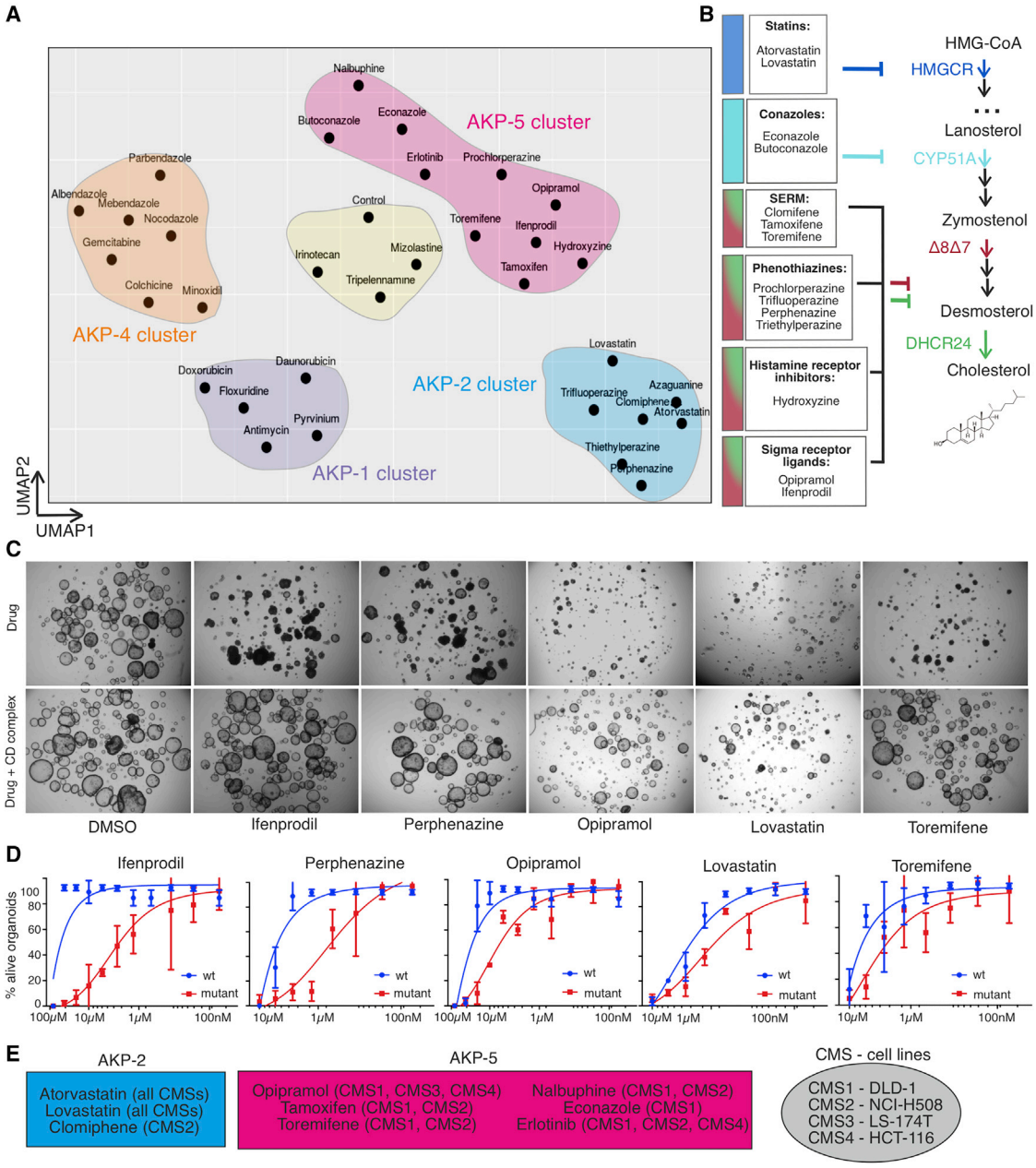

Figure 7. The mode of action of cancer organoid-targeting drugs is linked to the cholesterol biosynthesis pathway

(A) UMAP clustering of drug-treated AKP organoids. Color codes signify different clusters. UMAP is based on the expression of the most DE genes among AKP-treated samples. Cluster WT -3 is not present as glucocorticoids did not affect cancer organoids.

(B) Schematic representation of cholesterol biosynthesis pathway and drugs from statins and conazoles clusters targeting different enzymes of this pathway according to a literature search (see the reference list).

(C) Phase-contrast images of rescue of drug effects with cholesterol. CD, cholesterol:methyl-β-cyclodextrin (MβCD) complex (Christian et al., 1997).

(D) Drug response titration curves comparing WT (blue) and AKP mutant (red) treated organoids after 4 days of treatment.

(E) Colorectal cancer cell lines are targeted by drugs from AKP-2 (blue box) and AKP-5 (violet box) clusters. Right ellipse (gray) shows the assignment of these cell lines to a particular CMS.

- Targeted RNA-sequencing and data processing
- Analysis of published single-cell sequencing data
- FACS
- Whole mount immunofluorescence stainings
- Immunofluorescence, immunohistochemistry
- qPCR validation

● QUANTIFICATION AND STATISTICAL ANALYSIS

SUPPLEMENTAL INFORMATION

Supplemental information can be found online at https://doi.org/10.1016/j.celrep.2021.109026.

ACKNOWLEDGMENTS

This work was supported by grants from Carigest SA, Switzerland, and the ISREC Foundation, Switzerland, as well as by SNSF, Switzerland, grants. We thank T. Petrova (UNIL, Lausanne) and F. Radtke (EPFL Lausanne) for mouse strains, B. Mangeat (EPFL, Lausanne) for advice on library structure development, P. Dessen (EPFL, Lausanne) for growth factor production, A. Madurga Alonso (EPFL, Lausanne) for help in setting up FACS stains, L. Spisak (EPFL, Lausanne) for help in setting up immunofluorescence (IF) experiments, and C.M. Young (EPFL, Lausanne) for comments on the manuscript. We thank the EPFL core facilities, including GECF, BSF, HCF, BIOP, and FCCF, for their help during various parts of the project.

AUTHOR CONTRIBUTIONS

J.H. conceived the project. M.N. and J.H. designed the research and M.N. performed the experiments, established the bioinformatics pipelines, and performed the computational analysis, with contributions from J.H. P.O.-M. helped with organoid culture establishment and advised during the project. M.N. and J.H. prepared the manuscript, with input from P.O.-M.

DECLARATION OF INTERESTS

The authors declare no competing interests.

Received: August 8, 2020
Revised: December 22, 2020
Accepted: March 31, 2021
Published: April 20, 2021

REFERENCES

Adams, C.M., Goldstein, J.L., and Brown, M.S. (2003). Cholesterol-induced conformational change in SCAP enhanced by Insig proteins and mimicked by cationic amphiphiles. Proc. Natl. Acad. Sci. USA *100*, 10647–10652.

Basak, O., Beumer, J., Wiebrands, K., Seno, H., van Oudenaarden, A., and Clevers, H. (2017). Induced Quiescence of Lgr5+ Stem Cells in Intestinal Organoids Enables Differentiation of Hormone-Producing Enteroendocrine Cells. Cell Stem Cell *20*, 177–190.e4.

Basu, S., Cheriyamundath, S., and Ben-Ze'ev, A. (2018). Cell-cell adhesion: linking Wnt/β-catenin signaling with partial EMT and stemness traits in tumorigenesis. F1000Res. *7*, 1488.

Brown, S.S., Chen, Y.W., Wang, M., Clipson, A., Ochoa, E., and Du, M.Q. (2017). PrimerPooler: automated primer pooling to prepare library for targeted sequencing. Biol. Methods Protoc. *2*, bpx006.

Buczacki, S.J.A., Popova, S., Biggs, E., Koukorava, C., Buzzelli, J., Vermeulen, L., Hazelwood, L., Francies, H., Garnett, M.J., and Winton, D.J. (2018). Itraconazole targets cell cycle heterogeneity in colorectal cancer. J. Exp. Med. *215*, 1891–1912.

Bush, E.C., Ray, F., Alvarez, M.J., Realubit, R., Li, H., Karan, C., Califano, A., and Sims, P.A. (2017). PLATE-Seq for genome-wide regulatory network analysis of high-throughput screens. Nat. Commun. *8*, 105.

Butler, A., Hoffman, P., Smibert, P., Papalexi, E., and Satija, R. (2018). Integrating single-cell transcriptomic data across different conditions, technologies, and species. Nat. Biotechnol. *36*, 411–420.

Chen, S.H., Kuo, W.Y., Su, S.Y., Chung, W.C., Ho, J.M., Lu, H.H., and Lin, C.Y. (2018). A gene profiling deconvolution approach to estimating immune cell composition from complex tissues. BMC Bioinformatics *19* (*Suppl 4*), 154.

Christian, A.E., Haynes, M.P., Phillips, M.C., and Rothblat, G.H. (1997). Use of cyclodextrins for manipulating cellular cholesterol content. J. Lipid Res. *38*, 2264–2272.

Dekkers, J.F., Alieva, M., Wellens, L.M., Ariese, H.C.R., Jamieson, P.R., Vonk, A.M., Amatngalim, G.D., Hu, H., Oost, K.C., Snippert, H.J.G., et al. (2019). High-resolution 3D imaging of fixed and cleared organoids. Nat. Protoc. *14*, 1756–1771.

Feng, Y., Sentani, K., Wiese, A., Sands, E., Green, M., Bommer, G.T., Cho, K.R., and Fearon, E.R. (2013). Sox9 induction, ectopic Paneth cells, and mitotic spindle axis defects in mouse colon adenomatous epithelium arising from conditional biallelic Apc inactivation. Am. J. Pathol. *183*, 493–503.

Fumagalli, A., Oost, K.C., Kester, L., Morgner, J., Bornes, L., Bruens, L., Spaargaren, L., Azkanaz, M., Schelfhorst, T., Beerling, E., et al. (2020). Plasticity of Lgr5-Negative Cancer Cells Drives Metastasis in Colorectal Cancer. Cell Stem Cell *26*, 569–578.e7.

Gao, H., Korn, J.M., Ferretti, S., Monahan, J.E., Wang, Y., Singh, M., Zhang, C., Schnell, C., Yang, G., Zhang, Y., et al. (2015). High-throughput screening using patient-derived tumor xenografts to predict clinical trial drug response. Nat. Med. *21*, 1318–1325.

Gaujoux, R., and Seoighe, C. (2010). A flexible R package for nonnegative matrix factorization. BMC Bioinformatics *11*, 367.

Grün, D., Lyubimova, A., Kester, L., Wiebrands, K., Basak, O., Sasaki, N., Clevers, H., and van Oudenaarden, A. (2015). Single-cell messenger RNA sequencing reveals rare intestinal cell types. Nature *525*, 251–255.

Grün, D., Muraro, M.J., Boisset, J.C., Wiebrands, K., Lyubimova, A., Dharmadhikari, G., van den Born, M., van Es, J., Jansen, E., Clevers, H., et al. (2016). De Novo Prediction of Stem Cell Identity using Single-Cell Transcriptome Data. Cell Stem Cell *19*, 266–277.

Gu, Z., Eils, R., and Schlesner, M. (2016). Complex heatmaps reveal patterns and correlations in multidimensional genomic data. Bioinformatics *32*, 2847–2849.

Guinney, J., Dienstmann, R., Wang, X., de Reyniès, A., Schlicker, A., Soneson, C., Marisa, L., Roepman, P., Nyamundanda, G., Angelino, P., et al. (2015). The consensus molecular subtypes of colorectal cancer. Nat. Med. *21*, 1350–1356.

Haggar, F.A., and Boushey, R.P. (2009). Colorectal cancer epidemiology: incidence, mortality, survival, and risk factors. Clin. Colon Rectal Surg. *22*, 191–197.

Jackson, E.L., Willis, N., Mercer, K., Bronson, R.T., Crowley, D., Montoya, R., Jacks, T., and Tuveson, D.A. (2001). Analysis of lung tumor initiation and progression using conditional expression of oncogenic K-ras. Genes Dev. *15*, 3243–3248.

Karhausen, J., Furuta, G.T., Tomaszewski, J.E., Johnson, R.S., Colgan, S.P., and Haase, V.H. (2004). Epithelial hypoxia-inducible factor-1 is protective in murine experimental colitis. J. Clin. Invest. *114*, 1098–1106.

Kim, W.K., Kwon, Y., Jang, M., Park, M., Kim, J., Cho, S., Jang, D.G., Lee, W.B., Jung, S.H., Choi, H.J., et al. (2019). β-catenin activation down-regulates cell-cell junction-related genes and induces epithelial-to-mesenchymal transition in colorectal cancers. Sci. Rep. *9*, 18440.

Kolde, R. (2019). pheatmap: implementation of heatmaps that offers more control over dimensions and appearance. R package version 1.0.12. https://cran.r-project.org/web/packages/pheatmap/index.html.

Korade, Z., Kim, H.Y., Tallman, K.A., Liu, W., Koczok, K., Balogh, I., Xu, L., Mirnics, K., and Porter, N.A. (2016). The Effect of Small Molecules on Sterol Homeostasis: Measuring 7-Dehydrocholesterol in Dhcr7-Deficient Neuro2a Cells and Human Fibroblasts. J. Med. Chem. *59*, 1102–1115.

Langmead, B., Trapnell, C., Pop, M., and Salzberg, S.L. (2009). Ultrafast and memory-efficient alignment of short DNA sequences to the human genome. Genome Biol. *10*, R25.

Li, H. (2011). A statistical framework for SNP calling, mutation discovery, association mapping and population genetical parameter estimation from sequencing data. Bioinformatics *27*, 2987–2993.

Li, H., Handsaker, B., Wysoker, A., Fennell, T., Ruan, J., Homer, N., Marth, G., Abecasis, G., and Durbin, R.; 1000 Genome Project Data Processing Subgroup (2009). The Sequence Alignment/Map format and SAMtools. Bioinformatics *25*, 2078–2079.

Li, B., Flaveny, C.A., Giambelli, C., Fei, D.L., Han, L., Hang, B.I., Bai, F., Pei, X.H., Nose, V., Burlingame, O., et al. (2014). Repurposing the FDA-approved pinworm drug pyrvinium as a novel chemotherapeutic agent for intestinal polyposis. PLoS ONE *9*, e101969.

Li, H., Courtois, E.T., Sengupta, D., Tan, Y., Chen, K.H., Goh, J.J.L., Kong, S.L., Chua, C., Hon, L.K., Tan, W.S., et al. (2017). Reference component analysis of single-cell transcriptomes elucidates cellular heterogeneity in human colorectal tumors. Nat. Genet. *49*, 708–718.

Love, M.I., Huber, W., and Anders, S. (2014). Moderated estimation of fold change and dispersion for RNA-seq data with DESeq2. Genome Biol. *15*, 550.

Marino, S., Vooijs, M., van Der Gulden, H., Jonkers, J., and Berns, A. (2000). Induction of medulloblastomas in p53-null mutant mice by somatic inactivation of Rb in the external granular layer cells of the cerebellum. Genes Dev. *14*, 994–1004.

McInnes, L.H.J., and Melville, J. (2020). UMAP: Uniform Manifold Approximation and Projection for Dimension Reduction. arXiv, 1802.03426. http://arxiv.org/abs/1802.03426v3.

Miyamoto, S., Narita, T., Komiya, M., Fujii, G., Hamoya, T., Nakanishi, R., Tamura, S., Kurokawa, Y., Takahashi, M., and Mutoh, M. (2019). Novel screening system revealed that intracellular cholesterol trafficking can be a good target for colon cancer prevention. Sci. Rep. *9*, 6192.

Moebius, F.F., Striessnig, J., and Glossmann, H. (1997). The mysteries of sigma receptors: new family members reveal a role in cholesterol synthesis. Trends Pharmacol. Sci. *18*, 67–70.

Ootani, A., Li, X., Sangiorgi, E., Ho, Q.T., Ueno, H., Toda, S., Sugihara, H., Fujimoto, K., Weissman, I.L., Capecchi, M.R., and Kuo, C.J. (2009). Sustained in vitro intestinal epithelial culture within a Wnt-dependent stem cell niche. Nat. Med. *15*, 701–706.

Ordóñez-Morán, P., Dafflon, C., Imajo, M., Nishida, E., and Huelsken, J. (2015). HOXA5 Counteracts Stem Cell Traits by Inhibiting Wnt Signaling in Colorectal Cancer. Cancer Cell *28*, 815–829.

Sato, T., Vries, R.G., Snippert, H.J., van de Wetering, M., Barker, N., Stange, D.E., van Es, J.H., Abo, A., Kujala, P., Peters, P.J., and Clevers, H. (2009). Single Lgr5 stem cells build crypt-villus structures in vitro without a mesenchymal niche. Nature *459*, 262–265.

Schindelin, J., Arganda-Carreras, I., Frise, E., Kaynig, V., Longair, M., Pietzsch, T., Preibisch, S., Rueden, C., Saalfeld, S., Schmid, B., et al. (2012). Fiji: an open-source platform for biological-image analysis. Nat. Methods *9*, 676–682.

Schmitt, M., Schewe, M., Sacchetti, A., Feijtel, D., van de Geer, W.S., Teeuwssen, M., Sleddens, H.F., Joosten, R., van Royen, M.E., van de Werken, H.J.G., et al. (2018). Paneth Cells Respond to Inflammation and Contribute to Tissue Regeneration by Acquiring Stem-like Features through SCF/c-Kit Signaling. Cell Rep. *24*, 2312–2328.e7.

Schutgens, F., and Clevers, H. (2020). Human Organoids: Tools for Understanding Biology and Treating Diseases. Annu. Rev. Pathol. *15*, 211–234.

Schütte, M., Risch, T., Abdavi-Azar, N., Boehnke, K., Schumacher, D., Keil, M., Yildiriman, R., Jandrasits, C., Borodina, T., Amstislavskiy, V., et al. (2017). Molecular dissection of colorectal cancer in pre-clinical models identifies biomarkers predicting sensitivity to EGFR inhibitors. Nat. Commun. *8*, 14262.

Shibata, H., Toyama, K., Shioya, H., Ito, M., Hirota, M., Hasegawa, S., Matsumoto, H., Takano, H., Akiyama, T., Toyoshima, K., et al. (1997). Rapid colorectal adenoma formation initiated by conditional targeting of the Apc gene. Science *278*, 120–123.

Shim, J.S., Li, R.J., Lv, J., Head, S.A., Yang, E.J., and Liu, J.O. (2015). Inhibition of angiogenesis by selective estrogen receptor modulators through blockade of cholesterol trafficking rather than estrogen receptor antagonism. Cancer Lett. *362*, 106–115.

Simon, J.M., Paranjape, S.R., Wolter, J.M., Salazar, G., and Zylka, M.J. (2019). High-throughput screening and classification of chemicals and their effects on neuronal gene expression using RASL-seq. Sci. Rep. *9*, 4529.

Smith, T., Heger, A., and Sudbery, I. (2017). UMI-tools: modeling sequencing errors in Unique Molecular Identifiers to improve quantification accuracy. Genome Res. *27*, 491–499.

Tashiro, T., Okuyama, H., Endo, H., Kawada, K., Ashida, Y., Ohue, M., Sakai, Y., and Inoue, M. (2017). In vivo and ex vivo cetuximab sensitivity assay using three-dimensional primary culture system to stratify KRAS mutant colorectal cancer. PLoS ONE *12*, e0174151.

Teder, H., Koel, M., Paluoja, P., Jatsenko, T., Rekker, K., Laisk-Podar, T., Kukuškina, V., Velthut-Meikas, A., Fjodorova, O., Peters, M., et al. (2018). TAC-seq: targeted DNA and RNA sequencing for precise biomarker molecule counting. NPJ Genom. Med. *3*, 34.

Trapnell, C., Williams, B.A., Pertea, G., Mortazavi, A., Kwan, G., van Baren, M.J., Salzberg, S.L., Wold, B.J., and Pachter, L. (2010). Transcript assembly and quantification by RNA-Seq reveals unannotated transcripts and isoform switching during cell differentiation. Nat. Biotechnol. *28*, 511–515.

van de Wetering, M., Francies, H.E., Francis, J.M., Bounova, G., Iorio, F., Pronk, A., van Houdt, W., van Gorp, J., Taylor-Weiner, A., Kester, L., et al. (2015). Prospective derivation of a living organoid biobank of colorectal cancer patients. Cell *161*, 933–945.

Verissimo, C.S., Overmeer, R.M., Ponsioen, B., Drost, J., Mertens, S., Verlaan-Klink, I., Gerwen, B.V., van der Ven, M., Wetering, M.V., Egan, D.A., et al. (2016). Targeting mutant RAS in patient-derived colorectal cancer organoids by combinatorial drug screening. eLife *5*, e18489.

Voorneveld, P.W., Reimers, M.S., Bastiaannet, E., Jacobs, R.J., van Eijk, R., Zanders, M.M.J., Herings, R.M.C., van Herk-Sukel, M.P.P., Kodach, L.L., van Wezel, T., et al. (2017). Statin Use After Diagnosis of Colon Cancer and Patient Survival. Gastroenterology *153*, 470–479.e4.

Wages, P.A., Kim, H.H., Korade, Z., and Porter, N.A. (2018). Identification and characterization of prescription drugs that change levels of 7-dehydrocholesterol and desmosterol. J. Lipid Res. *59*, 1916–1926.

Wang, B., Rong, X., Palladino, E.N.D., Wang, J., Fogelman, A.M., Martín, M.G., Alrefai, W.A., Ford, D.A., and Tontonoz, P. (2018). Phospholipid Remodeling and Cholesterol Availability Regulate Intestinal Stemness and Tumorigenesis. Cell Stem Cell *22*, 206–220.e4.

Wei, T.S.V., Levy, M., Xie, Y., Jin, Y., and Zemla, J. (2017). corrplot: Visualization of a Correlation Matrix. https://cran.r-project.org/web/packages/corrplot/index.html.

Wiegering, A., Uthe, F.W., Hüttenrauch, M., Mühling, B., Linnebacher, M., Krummenast, F., Germer, C.T., Thalheimer, A., and Otto, C. (2014). The impact of pyrvinium pamoate on colon cancer cell viability. Int. J. Colorectal Dis. *29*, 1189–1198.

Ye, C., Ho, D.J., Neri, M., Yang, C., Kulkarni, T., Randhawa, R., Henault, M., Mostacci, N., Farmer, P., Renner, S., et al. (2018). DRUG-seq for miniaturized high-throughput transcriptome profiling in drug discovery. Nat. Commun. *9*, 4307.

Yin, X., Farin, H.F., van Es, J.H., Clevers, H., Langer, R., and Karp, J.M. (2014). Niche-independent high-purity cultures of Lgr5+ intestinal stem cells and their progeny. Nat. Methods *11*, 106–112.

Zhan, T., Ambrosi, G., Wandmacher, A.M., Rauscher, B., Betge, J., Rindtorff, N., Häussler, R.S., Hinsenkamp, I., Bamberg, L., Hessling, B., et al. (2019). MEK inhibitors activate Wnt signalling and induce stem cell plasticity in colorectal cancer. Nat. Commun. *10*, 2197.

STAR★METHODS

KEY RESOURCES TABLE

REAGENT or RESOURCE	SOURCE	IDENTIFIER
Antibodies		
mouse anti-L-FABP	Santa Cruz	sc-374537; RRID:AB_10990269
rat anti-Serotonin	Abcam	ab6336; RRID:AB_449517
mouse anti-ChrA	Santa Cruz	sc-393941; RRID:AB_2801371
donkey anti-mouse IgG Alexa 568	ThermoFisher Scientific	A-10037; RRID:AB_2534013
goat anti-mouse IgG Alexa 488	ThermoFisher Scientific	A-11029; RRID:AB_2534088
goat anti-rat IgG Alexa 568	ThermoFisher Scientific	A-11077; RRID:AB_2534121
donkey anti-rat IgG Alexa 488	ThermoFisher Scientific	A-21208; RRID:AB_2535794
Chemicals, peptides, and recombinant proteins		
human EGF Recombinant Protein	ThermoFisher Scientific	PHG0313
mouse R-spondin1 fusion to mouse Fc	Was produced and purified using a construct obtained from Dr. Calvin Kuo, Stanford University (Ootani et al., 2009)	mRspo1_mFc
mouse Noggin	The protein was produced and purified based on a cDNA that was synthetized according to NM_008711.2 followed by this linker and His tag (IEGRGGGSGGGSGGG SPGHHHHHHHH).	mNoggin_His
IWP-2	Stemgent	130-105-335
Gefetinib	Santa Cruz Biotechnology	sc-202166
CHIR99021	Sigma-Aldrich	SML1046-5MG
Valproic acid	Sigma-Aldrich	V0033000
Y-27632	Tocris	1254
DAPT	Sigma-Aldrich	D5942
Daunorubicin	Cayman chemical	CAY-14159-5
Atorvastatin	Sigma-Aldrich	PHR1422
Lovastatin	Adipogen Life Sciences	AG-CN2-0051-M025
Methyl-beta-cyclodextrin, average Mw 1310	Acros Organics	ACR37711-0050
Cholesterol	Adipogen Life Sciences	CDX-C0249-G025
DAPI for nucleic acid staining	Sigma-Aldrich	D9542
FITC Annexin V	Biolegend	640906
Peanut oil	Sigma-Aldrich	P2144
Tamoxifen	Sigma-Aldrich	T5648
Critical commercial assays		
Tth DNA-polymerase	Roche	11 480 022 001
Superscript II	Thermo Fisher Scientific	18064014
GoTaq G2 HS Polymerase	Promega	M7423
Oligo $d(T)_{25}$ magnetic beads	New England Biolabs	S1550S
Agencourt AMPure magnetic beads	Beckman Coulter Inc.	A63881
Magnetic mRNA Isolation Kit	New England Biolabs	S1550S
PowerUp SYBR Green Master Mix	Thermo Fisher Scientific	A25742
QIAquick Gel Extraction Kit	QIAGEN	28704
RNeasy Mini Kit	QIAGEN	74104

(*Continued on next page*)

Continued

REAGENT or RESOURCE	SOURCE	IDENTIFIER
Deposited data		
Gene expression profiles of treated organoids produced by TORNADO-seq	This paper	GEO: GSE157167
Experimental models: cell lines		
HCT-116	ATCC	CCL-247
DLD-1	ATCC	CCL-221
NCI-H508	ATCC	CCL-253
LS-174T	ATCC	CCL-188
Experimental models: organisms/strains		
$Lgr5^{GFP\text{-}IRES\text{-}CreER/+}$, C57BL/6J,	Jackson Laboratory	Stock No.: 008875
WT, C57BL/6J	Jackson Laboratory	Stock No.: 000664
$Cdx2^{CreERT2/+}$:APC^{lof}:$KRAS^{G12}$:$TP53^{lof}$, C57BL/6J	Jackson Laboratory	Stock No.; 022390, 009045, 008179, 008462
Oligonucleotides		
Rev primers for RT reaction, see Table S6	This paper	NA
Fw primers for 1st stage PCR, see Table S6	This paper	NA
Common rev primer for 1st stage PCR, see Table S6	This paper	NA
Primers for 2nd stage PCR (i5 index), see Table S6	This paper	NA
Primers for 2nd stage PCR (i5 index), see Table S6	This paper	NA
Software and algorithms		
FlowJo v10.7.1	FlowJo, LLC	https://www.flowjo.com/solutions/flowjo; RRID: SCR_008520
Oligoanalyzer	Integrated DNA Technologies	https://www.idtdna.com/calc/analyzer?c+US
ImageJ	(Schindelin et al., 2012)	Fiji, RRID:SCR_002285
Primer Pooler v1.41	(Brown et al., 2017)	http://ssb22.user.srcf.net/pooler/
BLAT	Jim Kent	https://genome.ucsc.edu
UMI-tools	(Smith et al., 2017)	https://github.com/CGATOxford/UMI-tools
Bowtie v1.2.2.	(Langmead et al., 2009)	http://bowtie-bio.sourceforge.net/index.shtml
Samtools v1.2.7	(Li et al., 2009; Li, 2011)	http://samtools.sourceforge.net
Cufflinks v2.2.1	(Trapnell et al., 2010)	https://github.com/cole-trapnell-lab/cufflinks
DESeq2	(Love et al., 2014)	10.1186/s13059-014-0550-8
pheatmap v1.0.12	(Kolde, 2019)	https://github.com/raivokolde/pheatmap
ComplexHeatmap v2.3.1.	(Gu et al., 2016)	10.18129/B9.bioc.ComplexHeatmap
umap v0.2.3.1.	(McInnes and Melville, 2020)	https://cran.r-project.org/web/packages/umap/
Nmf v0.21.0	(Gaujoux and Seoighe, 2010)	https://cran.r-project.org/web/packages/NMF/
mysort	(Chen et al., 2018)	https://testtoolshed.g2.bx.psu.edu/repository?repository_id=6e9a9ab163e578e0&changeset_revision=e3afe097e80a
corrplot v0.84	(Wei et al., 2017)	https://cran.r-project.org/web/packages/corrplot/

(*Continued on next page*)

Continued

REAGENT or RESOURCE	SOURCE	IDENTIFIER
Other		
Non-skirted PCR 96-well plate, for mRNA elution	Thermo Fisher Scientific	AB0600
V-bottom 96-well plate, for mRNA storage	PP Ratiolab	6018323
DynaMag - 96 Side magnet, for mRNA elution	Thermo Fisher Scientific	12331D
Magnetic Stand-96, for mRNA isolation	Thermo Fisher Scientific	AM10027
Low profile 96-well plates, for mRNA isolation	Thermo Fisher Scientific	AB-1127
96-well plates, for organoid growth	Grenier Bio-One	655090
Aluminum sealing	Corning	6570
Histogel	Thermo Fisher Scientific	HG-4000-012
Matrigel	Corning	356231

RESOURCE AVAILABILITY

Lead contact

Further information and requests for resources should be directed to and will be fulfilled by the Lead Contact, Joerg Huelsken (joerg.huelsken@epfl.ch).

Materials availability

This study did not generate new unique reagents.

Data and code availability

Gene expression profiles generated in this paper with TORNADO-seq has been deposited in the Gene Expression Omnibus (GEO) under accession number GEO: GSE157167. The files and the scripts for processing the raw data are deposited at https://github.com/MaximNorkin91/Tornado-seq-protocol/.

EXPERIMENTAL MODEL AND SUBJECT DETAILS

All experiments with mice were authorized by the Canton of Vaud (license VD3396) and were performed according to accepted guidelines for animal handling.

Mice

All mice were kept on a 12-hour light/dark cycle in individually ventilated cages. We used $Lgr5^{GFP\text{-}IRES\text{-}CreER/+}$ or wt mice for generation of normal intestinal organoids. The cancer organoids were generated from APC^{lof}:$KRAS^{G12}$:$TP53^{lof}$ mice. The $Apc^{fl/fl}$ mice (Shibata et al., 1997), $Kras^{Lsl\text{-}G12D}$ mice (Jackson et al., 2001) and $Tp53^{fl/fl}$ mice (Marino et al., 2000) were combined with $Cdx2^{CreERT2/+}$ mice (Feng et al., 2013) to obtain APC^{lof}:$KRAS^{G12}$:$TP53^{lof}$ intestinal tumors. All mice were in a C57BL/6 background. Healthy 8-10 weeks old male and female mice were used in the study. Mice used in this study had no previous history of drug administration, surgery or behavioral testing.

Cell lines

DLD-1 and NCI-H508 were cultured in RPMI 1640 media (61870010, Thermo Fisher Scientific). HCT-116 and LS-174T were cultured in DMEM-F12 media (31331-028, GIBCO). All cells were supplemented with 10% FBS (F7524, Sigma-Aldrich) and 1x pen strep (15140-122, GIBCO). Cells were passaged using Trypsin-EDTA (25300-054, GIBCO) every 2-3 days or when they reached 90% confluence. All cells were maintained in a 37°C, 5% CO2 atmosphere.

METHOD DETAILS

Organoid culture and drug screening

Organoid cultures were derived either from $Lgr5^{GFP\text{-}IRES\text{-}CreER/+}$ or wt mice as described previously (Sato et al., 2009). Cancer organoids were obtained by activating Cre-ERT2 in APC^{lof}:$KRAS^{G12}$:$TP53^{lof}$ mice. Cre-ERT2 was activated by a single intraperitoneal injection of tamoxifen dissolved in peanut oil (0.6 mg/ml) at a dose of 3 mg/kg. Six-month-old tumors were processed as follows: cut into small 2 mm pieces, washed thoroughly in PBS-EDTA at 4°C, then homogenized with a teflon pestle in 1.5 mL tubes. Tissue homog-

enates were trypsinized in Trypsin-EDTA for 3-4 min and quickly pipetted up and down, approximately 100-200 times, using 200 μl tips to disrupt any cell aggregates. After centrifugation, the pellets were resuspended in ENR media, filtered through 70 μm cell strainers (BD Bioscience) and single cell suspensions were mixed with cold Matrigel (Corning) and plated in 96-well plates. Organoids were cultured in 10 cm dishes in EGF, Noggin, and R-Spondin (ENR)-containing media for wt and AKP organoids. For the screening, organoids were physically disrupted by pipetting (50-100 times) until small clusters of cells or crypts were obtained and seeded at a concentration of 50 clusters/crypts per well of a 96-well plate. A selection of 320 drugs from a library of FDA-approved drugs was provided by the Biomolecular Screening Facility at EPFL. The drugs were applied 24h after organoid seeding at a final concentration of 10 μM (0.1% DMSO in ENR medium), organoids were treated for 2-4 days and harvested in 300 μl of lysis buffer (ref. S1550S, NEB). Two to four biological replicates were used in the screening. Chosen timing of the whole assay is long enough to be able to detect differentiation and short enough to avoid organoid starvation. The AKP model was selected as it reflects progression to a more advanced CRC stage. All wells of a 96-well plate were imaged using bright field microscopy (DMI4000b inverted microscope, Leica) prior to harvesting. Organoids were treated with published drug cocktails for 2 days (10 μM DAPT or 2 μM IWP-2, 1.5 mM VPA (DC1 – drug cocktail 1) or 3 μM CHIR99021, 1.5 mM VPA or 2 μM IWP-2, 10 μM DAPT, 5 μM Gefitinib (DC2 – drug cocktail 2)) according to previously established protocols for the primer validation experiments (Yin et al., 2014; Basak et al., 2017). These cocktails were used as positive controls in each separate 96-well experiment, along with untreated samples. Rescue experiments were performed with cholesterol:methyl-β-cyclodextrin (MβCD) complex (CD complex) at molar ratio of 1:8 with 242 μg/ml cholesterol and 5mM MβCD.

Targeted RNA-seq library construction

mRNA isolation

All library preparation steps were performed in 96-well plates. mRNA was isolated with The New England Biolabs (NEB) Magnetic mRNA Isolation Kit (S1550S) and the isolation was performed according to the manufacturer's protocol. Briefly, the media was removed by inverting and flicking the plate. For lysing the organoids, 200 μl of lysis buffer (S1550S, NEB) was added to each well using a multichannel pipette, Matrigel was disrupted by mechanical force using 200 μl tips and a multichannel pipette. Lysis buffer containing organoids was transferred to special 1.2 mL low profile plates (AB-1127, Thermo Fisher Scientific) and additional 100-200 μl of lysis buffer was added to each well. Organoids were disrupted by gently pipetting around 50 times. The 96-well plate was covered with aluminum sealing (6570, Corning) and put on a shaker at 300 rpm at RT for 10-15 min for efficient lysis. For mRNA binding, 22 μl of Oligo $d(T)_{25}$ magnetic beads (S1550S, NEB) was used. The mRNA isolation was performed according to the manufacturer's protocol using 200 μl of all wash buffers and 40-50 μl of elution buffer. A magnet (AM10027, Thermo Fisher Scientific, magnetic stand - 96) was used for separating the magnetic beads during the washes and a second magnet (12331D, Thermo Fisher Scientific, DynaMag - 96 Side) was used for separating the magnetic beads during the elution step. The mRNA-bead suspension was transferred to a non-skirted PCR plate (AB0600, Thermo Fisher Scientific) and incubated in a PCR machine at 55°C for 140 s prior to elution. Eluent was transferred to a V-bottom 96-well plate (6018323, 96-Well micro test plates, V-bottom, PP Ratiolab) and stored at −80°C.

RT reaction

RT reaction was carried out with Tth DNA-polymerase (11 480 022 001, Roche) according to the manufacturer's protocol in a non-skirted PCR plate (AB0600, Thermo Fisher Scientific) with 2.5 units of enzyme per reaction and 1 μl of a 0.5 μM mixture of gene specific reverse primers. Each reaction was pre-incubated at 72°C for 5 min without enzyme and then placed on ice. After the enzyme was added, the reaction was carried out at 72°C for 1 min and 60°C for 30 min. Obtained cDNA transcripts were cleaned with Agencourt AMPure magnetic beads (A63881, Beckman Coulter Inc.) according to the manufacturer's protocol at a 1:1.8 ratio of cDNA synthesis mixture:AMPure beads and eluted with 40 μl of elution buffer.

Amplification (1st and 2nd stage PCR)

Cleaned cDNA was used as a template for 1st stage PCR and amplified with GoTaq G2 HS Polymerase (M7423, Promega). 2 μl of purified cDNA, 1 μl of 5 μM 1st stage common primer and 1 μl of a 0.5 μM mixture of 206 forward primers were used (Table S6). The following PCR program was used - Table S7**.** Obtained products were purified with AMPure magnetic beads as described above. 2nd stage PCR was carried out with GoTaq G2 HS Polymerase, 1 μl of each 5 μM Fw and Rev 2nd stage indexing primers, 2 μl of purified 1st stage PCR product, and amplified for 15-20 cycles with the following program: 94°C - 20 s, 68°C – 15 s, 72°C – 10 s. Separately amplified libraries were pooled together by plates (96 samples) and purified twice on 2% agarose gels using QIAquick Gel Extraction Kit (28704, QIAGEN) according to the manufacturer's protocol.

Targeted RNA-sequencing and data processing

Pooled libraries were sequenced at an average depth of 70,000 reads per sample. Sequencing was performed on a NextSeq500 platform using a single-end (Read1 Illumina sequencing primer), standard depth 75 nt run at the Gene Expression Core Facility (EPFL, Lausanne, Switzerland). Custom index1 sequencing primer (PAGE purified) was added to the machine: 5′- act ctg cgt tga tac cac tgc ttc cgc gga cag gc −3′. Raw reads were first demultiplexed by standard Illumina protocols. The demultiplexed reads were processed with a custom script. Briefly, the first 10 bases of the each read contained UMI sequences and were deduplicated with UMI-tools. Deduplicated reads were processed with the Bowtie (ver. 1.2.2.)/samtools (ver. 1.2.7) pipeline and were aligned to a custom genome containing only the 206 target sequences. Aligned reads were counted with Cufflinks (ver. 2.2.1). The files and scripts for processing the raw data are deposited at https://github.com/MaximNorkin91/Tornado-seq-protocol/. Some samples

were excluded from the analysis due to technical errors using a threshold of 1000 total raw reads per sample. Obtained raw count tables were pre-processed for the analysis with DESeq2 package (ver. 1.24.0) in R. Batch effect correction was performed between 96-well plates: each sample was downscaled to 50000 reads and average gene expression per plate was calculated; scaling factor for each gene was calculated by dividing average gene expression value in one plate over average gene expression value in another plate . Normalization across the samples was performed based on the sample size (total counts per sample). Potential drug hits for the wt screen were determined as drugs altering more than 5 differentially expressed (DE) genes ($|log2FC| > 1$, $padj < 0.05$). The average Pearson's correlation for all compound hits using FC values was $r = 0.65$. Drugs inducing differentiation in wt or transformed organoids were defined as downregulating/upregulating 5 or more stem cell/differentiation genes (($|log2FC| > 1$, $padj < 0.05$) upon drug treatment. Heatmaps were obtained with pheatmap (ver. 1.0.12.) or ComplexHeatmap (ver. 2.3.1.) packages. Clustering was performed with umap (ver. 0.2.3.1.) and nmf (0.21.0) packages. Mysort toolbox in R was used to obtain cell type compositions. Correlograms were obtained with the corrplot (ver. 0.84) package. Figure 5A was obtained via the corrplot function in R by analyzing the 30 strongest (with more than 10 DE genes) drug hits. All genes with $|log2FC| > 1$ were used for obtaining specific up- and downregulated signatures. Figure 7A was obtained via the umap package in R using 40 most DE genes (significantly altered in at least 5 analyzed samples) between selected drugs for treated AKP organoids. Figure S7B was obtained with nmf package in R using the same criteria as in Figure 7A, for both wt and cancer treated organoids.

Analysis of published single-cell sequencing data

Single-cell RNA-sequencing data was obtained from GSE76408 and analyzed with StemID2 and Seurat packages in R according to published guidelines. For the analysis, 240 genes of interest were extracted from the file "transcript_counts_intestine_5days_YFP.xls." Cells were filtered based on a 100 reads threshold for the sum of these 240 gene counts; cells with fewer reads were discarded. Based on the results of the analysis and subsequent sequencing results 206 out of 240 genes were selected.

FACS

$Lgr5^{+}$ stem cells were sorted for the primer validation experiments. Intestinal crypts were isolated from 2-3 months old $Lgr5^{GFPiresCreER/+}$ mice as described previously (Sato et al., 2009). After several washes, the crypt cells were incubated with Trypsin-EDTA at 37°C for 5 min. Dead cells were excluded by DAPI staining. The GFP^{high} (Lgr5+) cells were sorted on a BD FACSAria Fusion at FCCF EPFL.

FITC AnnexinV (640906, Biolegend) and DAPI (D9542, Sigma-Aldrich) were used for detection of apoptotic and dead cells in human cell lines and were analyzed on the Attune NxT sorter. Cells in 96-well plates were trypsinized, washed with PBS and stained with AnnexinV antibody for 15 min in the dark (1:20 dilution), DAPI was added right before FACS analysis at 0.1 μg/ml. The results of this analysis are shown in Table S4; drugs which scored for inducing increased cell death were considered as relevant.

Whole mount immunofluorescence stainings

Whole mount stainings were performed as described (Dekkers et al., 2019) with few adjustments. In short, organoids were extracted from the wells by mechanical disruption of matrigel, sedimented by gravity to remove dead cells, and fixed for 1h in 4% PFA on ice. Tips precoated with 1% (wt/vol) BSA in PBS were used for handling. Fixed organoids were carefully washed with PBT buffer (0.1% (vol/vol) Tween in PBS) several times by aspirating the supernatant and adding 1ml of a fresh PBT solution, followed by an incubation for 10 min. Organoids were blocked in OWB buffer (0.1% (vol/vol) Triton X-100 and 0.2% (wt/vol) of BSA in PBS) for 15 min on ice and stained with primary antibodies (1:100-1:200 dilution) overnight at 4°C. Excess antibody was removed by washing several times with OWB buffer (3x30 minutes). Organoids were further incubated with secondary antibodies (1:500 dilution) for 4 hours at 4°C. After several washes organoids were resuspended in fructose-glycerol solution (pre-warmed to RT) and incubated for 20 min before embedding on slides as described previously. Imaging was performed on an inverted Leica SP8 confocal microscope and three-dimensional reconstructed confocal images were assembled in Fiji.

Immunofluorescence, immunohistochemistry

Organoids were extracted from at least 10 wells of a 48 well plate by mechanical disruption of the matrigel, sedimented by gravity to remove dead cells, and fixed overnight in 4% PFA on ice. Tips precoated with 1% (wt/vol) BSA in PBS were used for handling. Fixed organoids were carefully washed with PBT buffer (0.1% (vol/vol) Tween in PBS), mixed with pre-warmed Histogel (HG-4000-012, Thermo Fisher Scientific) and embedded in a final volume of 40 μl placed on the lid of a 10cm dish to solidify (4°C, 5 min). The Histogel drop containing the organoids was placed in the cassette and processed for dehydration and paraffin embedding according to standard procedures. Sections of 5-7 μm thickness were cut using a rotary microtome (Hyrax M25 V2) and dried at 60°C for 1h. After rehydration, antigen retrieval was performed by heat induced epitope retrieval (HIER) using pH 6.0 citrate buffer. Slides were washed with PBS (3x 5min). Organoid sections were surrounded with a hydrophobic barrier using a barrier pen and each section was incubated with a few drops of 1% BSA in PBS for blocking. Blocking solution was removed by tapping each slide several times. Sections were incubated with primary antibodies (1:100 – 1:400 diluted in 1% BSA in PBS) at 4°C overnight in a humidity chamber. Slides were washed in PBS (3x 5min) and incubated with the secondary antibody (1:1000 diluted in 1% BSA in PBS) for 1h at room temperature.

Slides were washed in PBS (3x 5min) and mounted in water-based Fluoromount media (0100-01, SoutherBiotech). Dehydration, rehydration procedures and antigen retrieval were performed at HCF, EPFL. Imaging was performed on a confocal microscope (Leica SP8 Inverted).

PAS staining was performed at HCF, EFPL, using standard protocols. Sirius Red staining was performed on rehydrated sections: 10 min Hematoxyline, 2 min tap water, 30 s (several dips) in 70% ethanol, 2h in Alkaline Sirius Red solution, rinsed with tap water, dried at room temperature and mounted in xylene based mounting media. Imaging was performed on an upright microscope (Leica DM5500 B).

The following primary and secondary antibodies were used: mouse anti-L-FABP (sc-374537, Santa Cruz), rat anti-SEROTONIN (ab6336, Abcam), mouse anti-CHGA (sc-393941, Santa Cruz), donkey anti-mouse Alexa 568 (A-10037, ThermoFisher Scientific), goat anti-mouse Alexa 488 (A-11029, ThermoFisher Scientific), donkey anti-rat Alexa 488 (A-21208, ThermoFisher Scientific), goat anti-rat Alexa 568 (A-11077, ThermoFisher Scientific).

qPCR validation

qPCRs during the validation step were performed with 50-100 organoids. RNA extraction was performed by two methods: with magnetic beads as described above and with a column-based method (74104, RNeasy Mini Kit, QIAGEN) for comparison of the results. Both RNA isolation procedures were performed according to the manufacturer's protocol. RT reaction from RNA samples isolated with the column-based method was performed with 50-500 ng of total RNA per reaction using either Superscript II (18064014, Thermo Fisher Scientific) or Tth DNA polymerase for comparison of the results. PowerUp SYBR Green Master Mix (A25742, Thermo Fisher Scientific) was used for qPCR amplification with 10 μl total volume per reaction and 0.5 μM final primer concentration. qPCR was performed in a StepOnePlus thermocycler (Applied Biosystems) and relative gene expression was determined by the comparative CT method based on expression of 6 housekeeping genes. A list of the primer sequences is provided in Table S6. Primers for qPCR comprise only the gene-specific part of the full-length primers for library construction from Table S6.

QUANTIFICATION AND STATISTICAL ANALYSIS

All statistical tests were executed using GraphPad Prism (Prism 7 for Mac OS X) software or the statistical software R (version 4.0.3). Mean with SD values are reported in the figures where qPCR validation, FACS or immunostaining quantifications were made. Differences between variables of control and treated samples were assessed by 2-tailed Student's t test.

2-4 biological replicates were used in organoid drug screening. Potential drug hits for the wt screen were determined as drugs altering more than 5 differentially expressed (DE) genes ($|log2FC| > 1$, $padj < 0.05$). Drugs inducing differentiation in wt or transformed organoids were defined as downregulating/upregulating 5 or more stem cell/differentiation genes (($|log2FC| > 1$, $padj < 0.05$) upon drug treatment.